J. DIFFERENTIAL GEOMETRY
28 (1988) 169-185

NEW MINIMAL SURFACES IN S^3

H. KARCHER, U. PINKALL & I. STERLING

Abstract

In this paper we construct new examples of compact imbedded minimal surfaces in S^3. We show some of these provide counterexamples to the conjecture that imbedded minimal surfaces separate S^3 into two domains of equal volume.

1. Introduction

We begin with the well-known tessellations of S^3 into cells having the symmetry of a Platonic solid in $\mathbf{R}^3$ and dihedral angle $2\beta_1$. Dividing a cell by its planes of symmetry we obtain as a fundamental region for the group of symmetries a tetrahedron with dihedral angles $\pi/2$, $\pi/2$, $\pi/2$, η, β_1, β_2 (see Table 1). The tetrahedron is determined by its dihedral angles.

TABLE 1

η, β_1, β_2	Cell Type	# of cells in tessellation	genus of constructed surfaces
$\pi/3, \pi/3, \pi/3$	Tetrahedral (Self-Dual)	5	6
$\pi/4, \pi/3, \pi/3$	Octahedral (Self-Dual)	24	73
$\pi/3, \pi/3, \pi/4$	Tetrahedral (or Cubical)	16(or 8)	17
$\pi/3, \pi/3, \pi/5$	Tetrahedral (or Dodecahedral)	600 (or 120)	601
$\pi/3, \pi/2, \pi/3$	Tetrahedral	2	3
$\pi/3, \pi/2, \pi/4$	Cubical	2	5
$\pi/3, \pi/2, \pi/5$	Dodecahedral	2	11
$\pi/4, \pi/2, \pi/3$	Octahedral	2	7
$\pi/5, \pi/2, \pi/3$	Icosahedral	2	19

To construct a minimal surface in S^3, we first find a minimal surface with boundary, called a "patch," within a tetrahedron (from Table 1) which intersects orthogonally all the plane-facrs of the tetrahedron in planar geodesics. From the patch we obtain a certain piece of the whole surface, called a "bone," by repeatedly reflecting "patches" through those plane-faces of the tetrahedron which are not contained in faces of the cell. Finally, we build the complete surface using reflections through faces of the cells (see Figures 1–3).[1]

Received October 16, 1986.

[1] All figures are stereographically projected to $\mathbf{R}^3$.

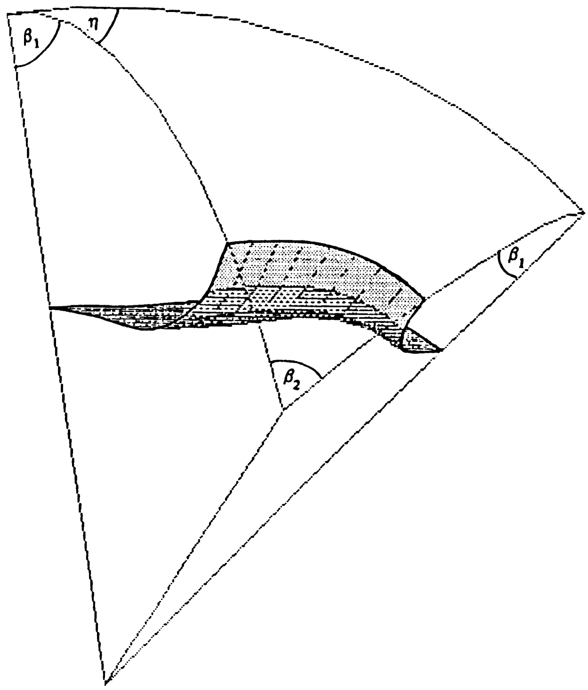

FIGURE 1

In §2 we outline our strategy of constructing the mentioned "patch." A similar construction has been used to obtain complete minimal surfaces in $\mathbf{R}^3$ [7, p. 66], [8] but in S^3 the arguments are more involved. The necessary control over the construction comes from lemmas based on the maximum principle (§3). This is enough to prove existence (§4). In §5 we get sufficient control on the polar minimal surface to prove that the "patch" is a graph in polar coordinates as in Figure 1; this implies imbeddedness.

Such imbedded minimal surfaces divide S^3 into two components whose volumes were conjectured to be always equal [9]. We have enough control on our surfaces to ensure in §5 that for some of them these two volumes are different.

For self-dual tessellations there is a simpler construction. In the case $(\pi/3, \pi/3, \pi/3)$ (resp. $(\pi/4, \pi/3, \pi/3)$) one solves the Plateau problem for the geodesic quadrilateral with all lengths $\pi/4$ (resp. $\pi/8$) and opposite angles equal $\pi/2$, $\pi/3$ (resp. $\pi/2, \pi/4$). Repeated reflections through the boundary geodesics directly yield the entire surface. One fifth (resp. one 24th) of this surface is a "bone" with boundary on a tetrahedral (resp. octahedral) cell (see Figures 4–5).

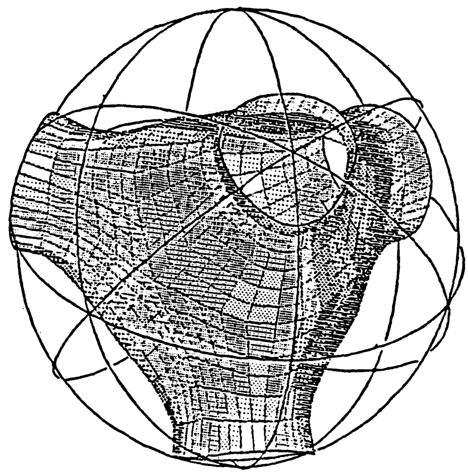

FIGURE 2

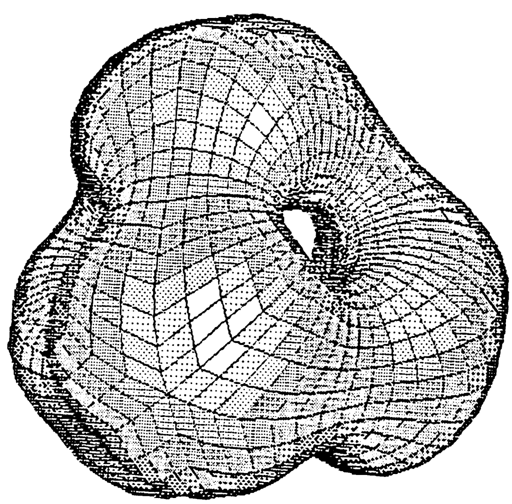

FIGURE 3

These simpler examples do separate S^3 into two components of equal volume. Indeed, the fact that these surfaces contain great circles implies that they separate S^3 into congruent components.

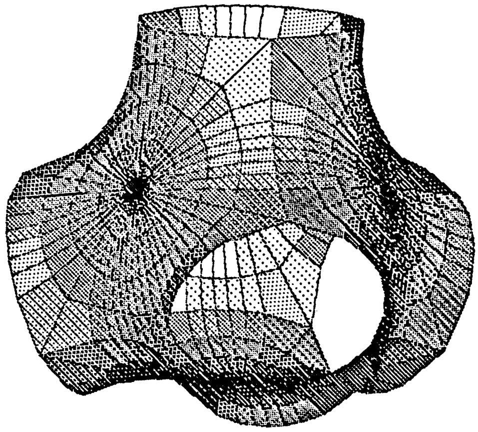

FIGURE 4

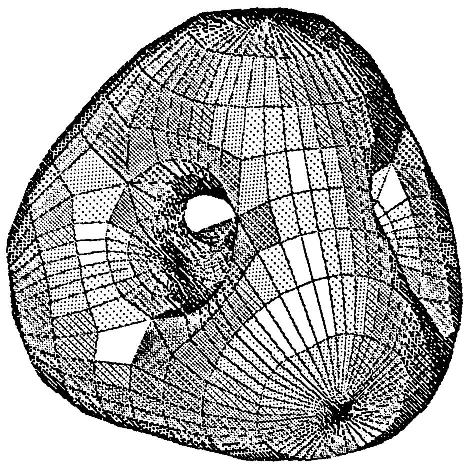

FIGURE 5

2. Outline of construction

We assume the results of [5], [6]. Explicitly we recall: The conjugate minimal surface M^* of a (simply connected) minimal surface M in a space of constant curvature is defined by giving its metric and Weingarten map (second fundmental tensor) as follows: $g^* = g$, $S^* = D^{90} \circ S$, where D^{90} is $90°$-rotation in the tangent spaces of M. Whenever necessary, η is fixed.

We want to find a minimal surface, in the fundamental tetrahedron, intersecting all faces perpendicularly and meeting those edges which have dihedral angles $\pi/2, \pi/2, \pi/2, \eta$. Such a patch is conjugate to a minimal surface bounded by a geodesic quadrilateral $ABCD$ with angles $\pi/2, \pi/2, \pi/2, \eta$

at A, B, C, D. Such quadrilaterals have two free parameters, e.g. the edge-lengths l_1, l_2 at A. The other two edge-lengths S_1, S_2 are determined by $\cos S_1 \cos l_1 = \cos S_2 \cos l_2$ and $\cos l_1 \cos l_2 = \cos S_1 \cos S_2 + \sin S_1 \sin S_2 \cos \eta$. (see Figure 6).

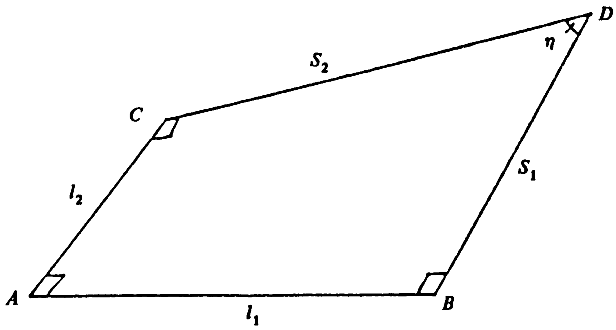

FIGURE 6

Let $M(\eta, l_1, l_2)$ denote the unique (§3) Plateau solution for any such geodesic quadrilateral. The conjugate minimal surface, denoted $M^*(\eta, l_1, l_2)$, determines by its planar boundary arcs a tetrahedron having, at the vertices A^*, B^*, C^*, D^* of this "patch", dihedral angles $\pi/2, \pi/2, \pi/2, \eta$. We have to choose l_1, l_2 in such a way that the other two dihedral angles are β_1, β_2 from Table 1. These dihedral angles are given as the angles between the normal planes at the endpoints of the (spherically) planar curves l_1^*, resp. l_2^*. These curves are determined by their geodesic curvature function $\kappa_i(\eta, l_1, l_2)$ $(i = 1, 2)$. We denote by $\alpha_i(\eta, l_1, l_2)$ the functions $\alpha_i(u)$ which give the turning angle between the totally geodesic plane through ABC and the tangent plane of $M(\eta, l_1, l_2)$ at the point on l_i which has distance u from A. Then $\kappa_i = \alpha_1'$ [5, p. 368].

In this way the dihedral angles β_1, β_2 are determined by the geodesic quadrilateral $Q = Q(\eta, l_1, l_2)$.

Note

$$\cos \alpha_1(B) = \frac{\cos l_1 \cdot \tan l_2}{\tan S_1} > 0, \quad \cos \alpha_2(C) = \frac{\cos l_2 \cdot \tan l_1}{\tan S_2} > 0.$$

From [6, Theorem 2] and from the argument in [5, p. 350] we have

Lemma 1. *The Plateau solution $M(\eta, l_1, l_2)$ is contained in the convex hull $C(Q)$ of the boundary quadrilateral. The intrinsic curvature of M is less than 1, except at D; therefore, all the turning angle functions of the four edges are strictly monotone. Hence, also, $l_1^*, l_2^*, S_1^*, S_2^*$ are locally convex.*

The Frenet frame x, t, n of the curve l_i^* is controlled by the Frenet equations

$$(1) \qquad \begin{cases} x' = t, \\ t' = -x + \kappa n, \\ r' = -\kappa t, \end{cases} \quad \text{or} \quad \begin{cases} x' = a \cdot \cos\alpha + b \cdot \sin\alpha, \\ a' = -x \cdot \cos\alpha, \\ b' = -x \cdot \sin\alpha, \end{cases}$$

where $\alpha = \alpha_i(\eta, l_1, l_2)$, $\kappa = \alpha'$, $a = t \cdot \cos\alpha - n \cdot \sin\alpha$ and $b = t \cdot \sin\alpha + n \cdot \cos\alpha$. Observe $\beta_i = \cos^{-1}\langle t(l_i), t(0)\rangle$.

The second version of the Frenet equations does not need the derivative of the turning angle function α. This will allow us to prove continuity of the map $(\beta_1, \beta_2) := F_\eta(l_1, l_2)$ and to establish sufficiently narrow bounds which imply that the (β_1, β_2)-pairs of Table 1 are in the range of F_η—thus establishing existence of all the patches.

3. The maximum principle and basic lemmas

Maximum principle [7]. *Suppose that M_1, M_2 are two branched minimal surfaces such that for a point $p \in M_1 \cap M_2$ the surface M_1 locally lies on one side of M_2 near p. Then the surfaces M_1, M_2 coincide near p.*

We have already quoted from Lawson [6] that a minimal surface contained in an open half-sphere actually is contained in the convex hull of its boundary—because, for equator spheres S, it is clear what is meant by "M lies on one side of S." We wish to use the following ruled minimal surfaces ("helicoids") as comparison surfaces in the maximum principle.

A helicoid with constant turning speed τ is given as follows: Let $c(s)$ be a geodesic (called an axis) and $e_1(s)$, $e_2(s)$ orthonormal parallel fields along c. Then

$$H(s,t) := \exp_{c(s)} t \cdot (e_1(s)\cos(\tau \cdot s) + e_2(s) \cdot \sin(\tau \cdot s)),$$

$(0 \le s \le l,\ 0 \le t \le \pi/2)$. The tangent turning angle along the rulings is not constant, but is given by $\tan\alpha(t) = \tau \cdot \tan t$. ($\tau = 1$ gives the Clifford torus and $\tau = 2$ gives Lawson's Klein bottle.)

The orbits of the rotation around c are transversal to the helicoid except on c and its polar circle. We will choose helocoids having as an axis one of the edges l_1, l_2 of the quadrilateral Q and with the property that the convex hull $C(Q)$ can be rotated around the axis to a position where it meets the helicoid only along the axis.

Then we have an:

Extended maximum principle. *If one rotates the Plateau solution, M, of Q in either direction around the axis, then M first meets the helicoid (excluding the axis) at a boundary point. (This is also true in euclidean geometry.)*

The same sort of "extended maximum principle" will be applied below also to other comparison surfaces than helicoids.

Proof. Directly by the maximum principle the helicoid and M cannot first meet at an interior point. We have to exclude the case that the Plateau solution first becomes tangential to the helicoid at interior points of the axis and not at the endpoints. To do so we choose an auxiliary axis $\bar{c}$ in such a common tangent plane by extending the touching ruling to $t = -\varepsilon$ and choose $\bar{c}$ perpendicular to the rule. Now continue the rotation of M around c a little further and rotate back around $\bar{c}$. In this way the Plateau solution can be moved to touch the helicoid from one side at an interior point $-$a contradiction. q.e.d

There is an optimal choice of such comparison helicoids due to the following: If one describes the edge S_1 (resp. S_2) in helicoidal coordinates with the axis l_2 (resp. l_1) one finds convex turning angle functions $\tilde{\alpha}(u)$ given by $\tan\tilde{\alpha}(u) = (\tan\alpha(l)/\tan l)\cdot\tan u$, $0 \le u \le l$ (note: $l_i < \alpha(l_i) < \pi/2$). The secant of $\tilde{\alpha}(u)$ has slope $\underline{\tau} = \alpha(l)/l$, the initial tangent of $\tilde{\alpha}(u)$ has slope $\bar{\tau} = \tan\alpha(l)/\tan l$. These are the optimal constant turning speeds for helicoids (axis l_i) which touch the quadrilateral from one side or from the other. Because of our extended maximum principle, they leave the Plateau solution on one side. Our notations are such that α_2 is increasing, and α_1 is decreasing. We therefore get lower bounds for α_2 (resp. $-\alpha_1$) from the two helicoids with axis l_i and turning speed $\underline{\tau}_i$, and upper bounds with $\bar{\tau}_i$ $(i = 1, 2)$.

$$\begin{aligned}
&\alpha_2^{1L}(u) = \tan^{-1}(\underline{\tau}_1\cdot\tan u),\\
&\alpha_2^{2L}(u) = \underline{\tau}_2\cdot u \text{ (the secant of the function } \alpha_2),\\
(2)\qquad &\alpha_2^{1U}(u) = \tan^{-1}(\bar{\tau}_2\cdot\tan u),\\
&\alpha_2^{1U}(u) = \bar{\tau}_1\cdot u \text{ (the initial tangent of } \alpha_2),\\
&\text{similar formulas hold along } l_1.
\end{aligned}$$

We summarize this as

Lemma 2. $\alpha_i^{jL}(u) \le \alpha_i(u) \le \alpha_i^{jU}(u)$, $0 \le u \le l_i$ $(i, j = 1, 2)$.

Lemma 3. *Any minimal surface with boundary Q and in the convex hull of Q is the unique Plateau solution.*

Proof. Since Q has geodesic edges, we can extend the minimal surfaces by 180°-rotation to a rim around the quadrilateral. Since the turning angles α_i are less than $\pi/2$ one can rotate a second copy of the convex hull by 180° around l_i so that the two copies meet only along the edge l_i. Having two different minimal surfaces bounding Q and in the convex hull clearly contradict our extension of the maximum principle.

Lemma 4. *The function $(\beta_1, \beta_2) = F_\eta(l_1, l_2)$ is continuous.*

Proof. Given ε we rotate Q around l_1 (resp. l_2) by ε. A sufficiently small change of l_1, l_2 in the rotated position will leave the changed quadrilateral on one side of M. Again, by the extended maximum principle, this proves the new turning functions are in an ε-strip around the initial α_i's. The second version of the Frenet equations now shows that the β_i's change correspondingly little.

4. Existence

Lemma 5. *Let $s \mapsto x(s)$, $s \mapsto \underline{x}(s)$, and $s \mapsto \bar{x}(s)$, $0 \le s \le l$ be three locally convex arcs on S^2, of the same length $l < \pi/2$. Let $\kappa, \underline{\kappa}$ and $\bar{\kappa}$ denote the corresponding geodesic curvatures, (x,t,n), $(\underline{x}, \underline{t}, \underline{n})$, and $(\overline{x}, \bar{t}, \overline{n})$ the corresponding Frenet-frames with* $\det(x,t,n) = 1$, $\underline{\alpha}(u) = \int_0^u \kappa(s)\,ds$ *the integrated curvatures, etc. Assume for all s*

$$\underline{\alpha}(s) \le \alpha(s) \le \overline{\alpha}(s) < \pi/2. \tag{3}$$

Then

(a) $\langle \underline{x}(s),\ \underline{t}(0)\rangle \ge \langle x(s),\ t(0)\rangle \ge \langle \bar{x}(s),\ \bar{t}(0)\rangle$ *for all s,*

(b)

$$\begin{aligned}
&\cos\alpha(l) - \int_0^l \cos(\alpha(l) - \bar{\alpha})\langle \underline{x}(s), \underline{t}(0)\rangle\,ds \\
&\le \langle t(l), t(0)\rangle \\
&\le \cos\alpha(l) - \int_0^l \cos(\alpha(l) - \underline{\alpha})\langle \bar{x}(s), \bar{t}(0)\rangle\,ds.
\end{aligned}$$

Proof. (b) follows easily from (1), (3) and (a) by using

$$-(\cos\alpha(l)\cos\alpha + \sin\alpha(l)\sin\alpha) = -\cos(\alpha(l) - \alpha) \le -\cos(\alpha(l) - \underline{\alpha}),$$

etc. To prove (a) we first show

$$\begin{array}{lll}
\langle x(s), x(0)\rangle > 0 & \langle t(s), x(0)\rangle < 0 & \langle n(s), x(0)\rangle > 0 \\
\langle x(s), t(0)\rangle > 0 & \langle n(s), t(0)\rangle < 0 & \\
\langle x(s), n(0)\rangle > 0 & \langle t(s), n(0)\rangle > 0 & \langle n(s), n(0)\rangle > 0 \\
\langle x(s) \times x(t), t(0)\rangle > 0 & \text{for } t > s \text{ (see Figure 7).} &
\end{array} \tag{4}$$

Remark. These inequalities imply that x and n are convex (not only locally convex).

By the Frenet equations, (4) clearly holds for small $s > 0$. It is therefore sufficient to see that none of the scalar products in (4) can become zero for $s > 0$. In the cases $\langle x(s), x(0)\rangle$ and $\langle n(s), n(0)\rangle$, this follows from the fact that the curves x and n have lengths l and $\alpha(l)$ respectively, both being less than $\pi/2$.

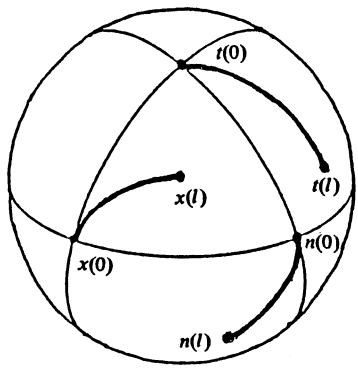

FIGURE 7

The tangent great circle of the curve x never passes through the point $n(0)$, because then we would have $\langle n(s), n(0)\rangle = 0$. This together with the local convexity of x implies our inequality (4) involving $x(s)$. A similar argument (note that also n is a locally convex curve with curvature $1/\kappa$) implies the assertions in (14) about $n(s)$.

The geodesic segment from $x(s)$ to $n(s)$ cuts the great circle polar to $t(0)$ in a point y satisfying $\langle y, x(0)\rangle > 0$, $\langle y, n(0)\rangle > 0$. This implies our claims about $t(s) = x(s) \times n(s)$, proving all of (4) (and the remark following (4)).

Secondly, given $\varepsilon > 0$, one may choose step functions $\underset{\sim}{\alpha}, \tilde{\alpha}$ such that

$$(5) \qquad \alpha(s) - \varepsilon \le \underset{\sim}{\alpha}(s) \le \alpha(s) \le \tilde{\alpha}(s) \le \alpha(s) + \varepsilon.$$

The corresponding $\tilde{x}, \underset{\sim}{x}$ given by the second version of the Frenet equations (1) are then close to x in the sense that $\lim_{\varepsilon\to 0} \tilde{x}, \underset{\sim}{x} = x$.

Therefore it suffices to prove (a) for the case where $\underline{x}, x$, and $\bar{x}$ are all polygons. We work now with $\underline{x}$ and x, the case of x and $\bar{x}$ is similar. By subdividing we can assume that the vertices of x and $\bar{x}$ correspond to the same parameter values $0 = s_n < s_{n-1} < \cdots < s_1 < s_0 = l$. We define a one-parameter family of polygons x_λ, $0 \le \lambda \le n$, $x_0 = x$, $x_n = \bar{x}$ corresponding to the integrated curvature functions α_λ defined inductively on v as follows: $\alpha_0 = \alpha$ and for $\lambda = v + d$, $v \in \{0, \cdots, n-1\}$, $0 < d \le 1$, we set

$$(6) \qquad \alpha_\lambda(s) = \begin{cases} \alpha_v(s) & \text{for } s \notin (s_{v+1}, s_v], \\ (1-d)\alpha_v(s) + d\bar{\alpha}(s) & \text{for } s \in (s_{v+1}, s_v]. \end{cases}$$

All α_λ are nondecreasing, so the polygons x_λ are convex, and hence the inequalities (4) are available for x_λ. To compare polygons for different λ, we assume, with the obvious notation,

$$(7) \qquad x_\lambda(0) = x(0), \quad t_\lambda(0) = t(0), \quad n_\lambda(0) = n(0)$$

for all λ. Using this we will prove

$$\frac{d}{d\lambda}\langle x_\lambda(s), t(0)\rangle \le 0 \quad \text{for } \lambda \notin \mathbf{Z}, \tag{8}$$

and for every fixed s. This, obviously, will complete the proof.

(6) means that the function α_λ is fixed except on the interval $(s_{v+1}, s_v]$ where it is moving upward at a constant speed (see Figures 8 and 9). For the corresponding polygon x_λ, this means that the angle at the vertex $x(v)$ is increasing at a certain rate, while the angle at $x(v+1)$ is decreasing at the same rate.

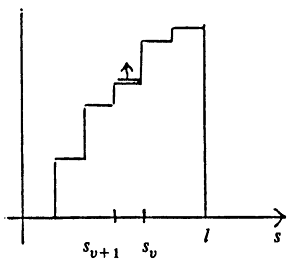

FIGURE 8

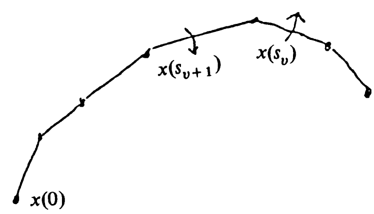

FIGURE 9

Clearly then, the last inequality (4) implies (8) for $s \in (v, v+1]$; and thus (since points $x_\lambda(s)$ for $s \le s_v$ are not moving at all) for $s \le s_{v+1}$. The increasing kink at $x_\lambda(s_v)$ imposes on all $x_\lambda(s)$, $s > s_v$, an infinitesimal rotation with angular velocity vector $\omega = -cx_\lambda(s_v)$ for some constant $c > 0$. The decreasing kink at $x_\lambda(s_{v+1})$ induces a rotation with $\omega = cx_\lambda(s_{v+1})$. The linearity of the Frenet equations implies that the total effect on $x_\lambda(s)$, $s > s_{v+1}$, is an infinitesimal rotation with angular velocity

$$\begin{aligned} \omega &= c(x_\lambda(s_{v+1}) - x_\lambda(s_v)) \\ &= \tilde{c}t_\lambda(s) \quad \text{for some } s \in (s_{v+1}, x_v]. \end{aligned} \tag{9}$$

$\tilde{c} > 0$, together with the information in (4), then yields (8).

Theorem. *The minimal surfaces listed in Table* 1 *exist*; *more specifically: for all η, β_1, β_2 of Table* 1 *there exist (l_1, l_2) such that $F_\eta(l_1, l_2) = (\beta_1, \beta_2)$.*

Proof. The idea is to find a contractible curve $l(s) = (l_1(s), l_2(s))$ such that the curve $F_\eta(l(s))$ has nonzero winding number around the point (β_1, β_2) (see Figures 10 and 11).

This is easy for the third and fourth examples of Table 1 (see Figure 12): Along $\cos l_1 \cos l_2 = \cos\eta$ we have $\pi/2 = \alpha_i \le \beta_i$ $(i = 1, 2)$. Along the other three parts we have $\lim_{\varepsilon\to 0} \beta_i = \alpha_i$; the small circle corresponds to the euclidean limit where $\cos\eta = \sin\alpha_1 \cdot \sin\alpha_2$, and on the two straight portions

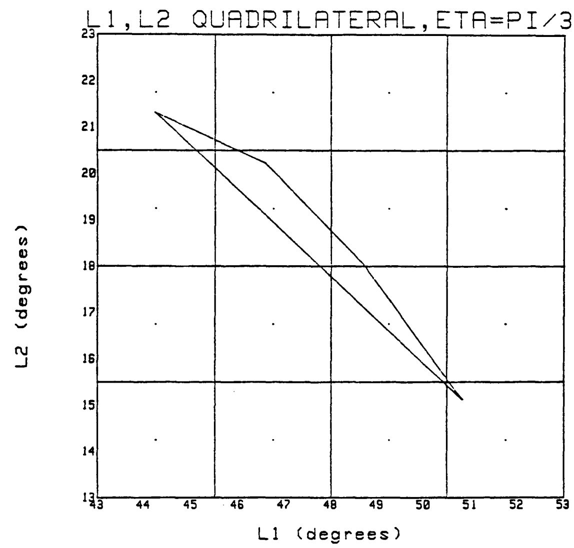

FIGURE 10

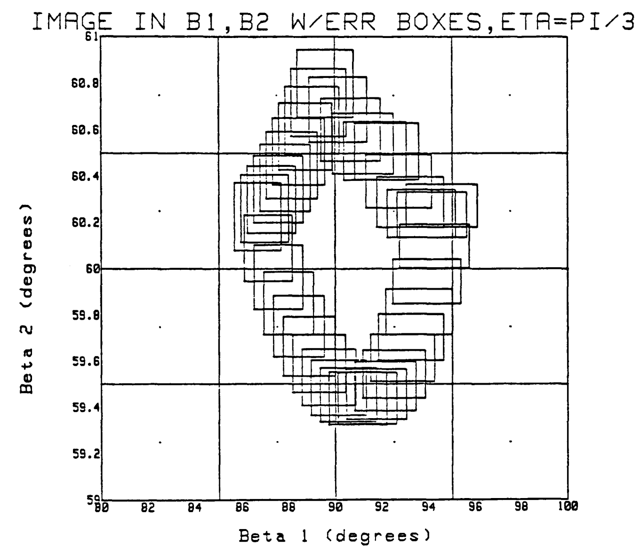

FIGURE 11

we have: $l_2 \to 0$ (resp. $l_1 \to 0$) implies $\alpha_1 \to \pi/2$ (resp. $\alpha_2 \to \pi/2$) (this also works for the first and second examples of Table 1 which were discussed separately in §1).

The remaining five examples are obtained with some numerical help based on (b) of Lemma 5. Recall that $\underline{\alpha}(s), \bar{\alpha}(s)$ are explicit function given in Lemma

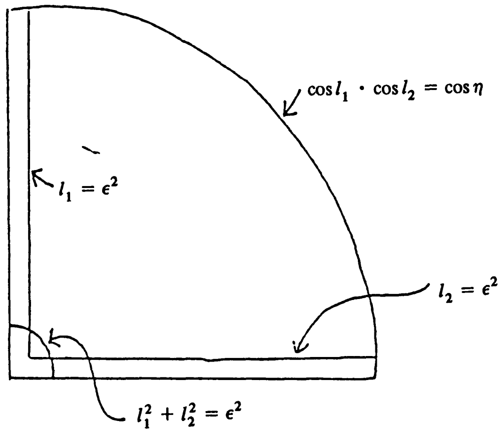

FIGURE 12

2. The corresponding $\underline{x}(s), \bar{x}(s)$ are either circles if $\alpha = \text{const.}$ or meridians of minimal surfaces of revolution in S^3 which are given explicitly in [1, p. 25] in terms of elliptic integrals; of course they are also given as solutions of the Frenet equations (1).

For any η, l_1, l_2 we have the bounds $\underline{\alpha}(s)$, $\bar{\alpha}(s)$ of Lemma 2 for the turning angle functions $\alpha(s)$ of $M(\eta, l_1, l_2)$. Lemma 5(b) applied to these explicit bounds and their corresponding Frenet curves gives, through one more integration, bounds $\underline{\beta}_i \leq \beta_i \leq \bar{\beta}_i$ $(i = 1, 2)$, which are shown as boxes in Figure 11. For this last step we rely on numerical integration. The data then show that the continuous center curve of the boxes surrounds the desired (β_1, β_2)-value at such a distance that it is outside all the error boxes. Since the curve $F_\eta(l(s))$ stays in these error boxes, its winding number with respect to (β_1, β_2) is nonzero. q.e.d

Note that beyond existence the above method gives also a certain region R, in (l_1, l_2)-space, in which our desired (l_1, l_2)-value must lie. Combined with our knowledge about the boundary curve of the patch M^* (see Lemmas 2 and 5) this allows us to obtain pictures of the stereographic projections of our surfaces which are qualitatively correct (see Figures 3 and 13–16).

5. Polar varieties, imbeddedness, and volume estimates

Let M^P be the polar variety of $M = M(\eta, l_1, l_2)$, defined by going a distance $\pi/2$ in the normal direction from M. It is again a minimal surface. The polar surface of M^P is again M. Let Q^P be its boundary, etc.

Lemma 6. $M^P \subset C(Q^P)$.

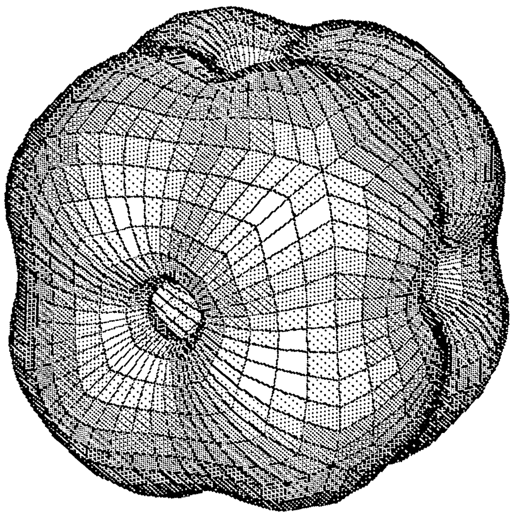

FIGURE 13

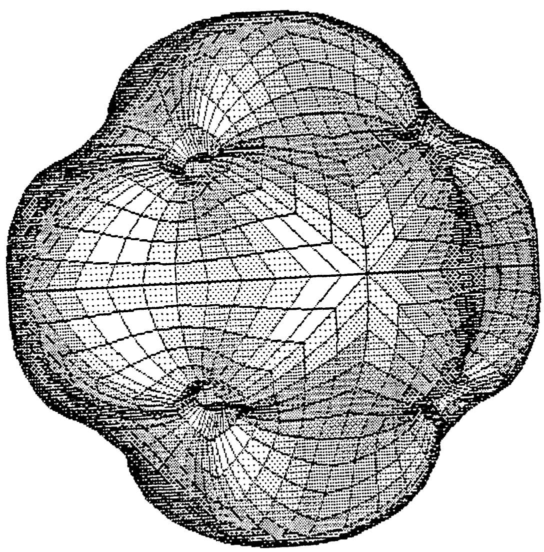

FIGURE 14

Proof. Let Π=plane (A^P, B^P, C^P)=polar plane of A=equator sphere in spherical polar coordinates centered at A. Poles of "vertical" (i.e. passing through A) planes in this coordinate system lie in Π. Since no points of $M = (M^P)^P$ lie in Π, no tangent planes of M^P are vertical (in particular, M^P does not pass through A or $-A$). Now project M^P to Π. This gives a

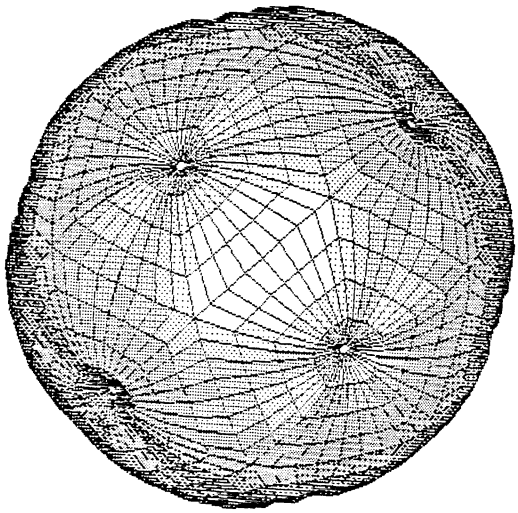

FIGURE 15

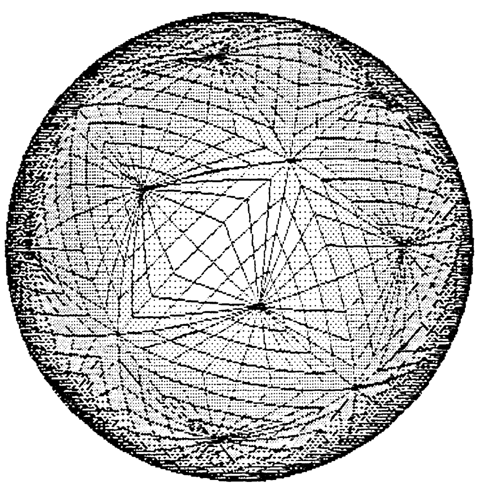

FIGURE 16

local homeomorphism $f\colon M^P \to \Pi$ and the boundary curves project one-to-one to Π. Therefore, f is a homeomorphism onto the "interior" component of $\Pi = f(Q^P)$. So $M^P \subset f^{-1}(f(M^P))$ (= a spindle with cross section Q^p), which is contained in an open hemisphere of S^3. The lemma then follows by [6, Theorem 1].

Note. By the same argument as in Lemma 3, M^P is unique and hence it is the Plateau solution of Q^P.

Lemma 7. $M^* = M^*(\eta, l_1, l_2) \subset C(Q^*)$ (*resp.* $M^{*P} \subset C(Q^{*P})$).

Proof. By [6, Theorem 1], together with the fact that M (resp. M^P) is isometric to M^* (resp. M^{*P}), it suffices to show that the intrinsic distances from some point in M (resp. M^P) are less than π. The circumference of Q, $l_1+l_2+S_1+S_2$, is less than $4\cdot\pi/2$. Two edges of Q^P are α_1, α_2, which are both less than $\pi/2$, and since $\eta^P = 180 - \eta$, we also have S_1^P, S_2^P both less than $\pi/2$. Since M and M^P are Plateau discs we have, using two triangles, their areas bounded less than π. Hence for any piece of them $\int K\, dA \leq \int dA < \pi$. Consequently there are no geodesic loops. Then, the same argument as [3, p. 108] shows that any two points of M (resp. M^P) are connected by a unique geodesic in M (resp. M^P) shorter than π. Since a minimal surface in S^3 has its intrinsic curvature ≤ 1, we can now apply the Alexandrov angle comparison theorem to the geodesic triangles formed by two adjacent edges of Q (resp. Q^P) and an intrinsic diagonal [9, Cor. 6.4.3]. In particular, all geodesic secants from any vertex of $Q(Q^P)$ to the opposite diagonal are shorter ($\leq$) then the longest edge of $Q(Q^P)$, hence $< \pi/2$. The geodesic triangles formed by one edge of $Q(Q^P)$ and the segments to the midpoint of either diagonal have all their edge lengths $< \pi/2$, hence their intrinsic diameter $< \pi/2$. The lemma follows.

Lemma 8. *For all* (η, β_1, β_2) *in Table* 1, *the surface generated by* $M^*(\eta, \beta_1, \beta_2)$ *is embedded.* (*Compare Figure* 1).

Proof. For simplicity, we consider the case $(\pi/3, \pi/2, \pi/3)$ in detail; the other cases are similar. First, stereographically project so that the plane Π_2^* containig l_2^* goes to S^2 and now work in $\mathbf{R}^3$. $C(Q^{*P}) \cap S^2 = l_2^{*P}$. Any "vertical" plane (i.e. vertical to S^2) in spherical polar coordinates around 0 must have its normal on S^2. However, by Lemma 7, any interior normal to M^* lies outside S^2. Thus M^* is a graph in these coordinates, and the lemma follows. q.e.d

It was proved by Lawson that a compact minimal imbedded surface in S^3 separates S^3 into two diffeomorphic components. The following conjecture is attributed to Lawson [9, p. 692].

Conjecture. *Any compact imbedded minimal surface in* S^3 *separates* S^3 *into two components of equal volume.*

The surface generated by $M(\pi/3, \pi/2, \pi/5)$ is a counterexample.

It suffices to prove M stays within a distance $\pi/2 - D$ ($\approx 23,8°$) of its equator of reflections, E, where $4D - 2\sin(2D) = \pi$, since this tube around E contains half the volume of S^3.

By the analysis in the proof of Lemma 8, the maximum distance from E must occur on S_1^*. By Lemma 1, and the remark following equations (4), S_1^* is convex. Hence it suffices to check that $\bar{h} = \pi/2 - \sin^{-1}\{\tan(|S_1^*|)/\tan\phi\}$ is less than $\pi/2 - D$, where ϕ is given by $\cos\beta_1 = \sin\eta\cos\phi$.

Finally, by the Theorem, we know (l_1, l_2) lies within a certain region R in (l_1, l_2)-space (e.g. here $.54 < l_1 < .56$, $.01 < l_2 < .03$). This gives $\max_{(l_1,l_2)\in R} \bar{h} < 15° < \pi/2 - D$ (the actual value is approximately 7°) (see Figure 17).

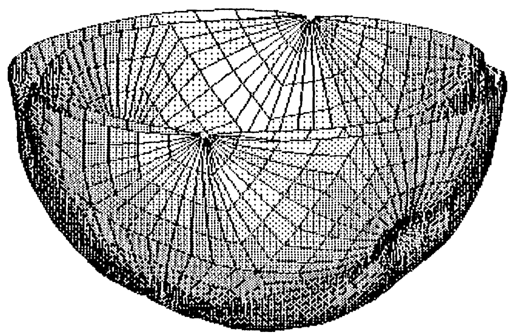

FIGURE 17

Remark. Computer estimates indicate the area of Lawson's three-hold torus $\xi_{1,3}$ is less than that of the genus three surfaces generated by $M(\pi/3, \pi/2, \pi/3)$. This lends evidence to Kusner's conjecture [3] that stereographic projections of Lawson's n-holed tori $\xi_{1,n}$ are "optimal," in the sense that they are absolute minima of the Willmore integral, $\int H^2\, dA$, among all genus n surfaces. Similarly, Lawson's Klein bottle $\tau_{1,2}$ at present is also a candidate to be "optimal" (see Figures 18 and 19).

Added in proof. Lawson showed [5, p. 365]: If g, S are the metric and Weingarten map of a minimal surface in a space of constant curvature $\tilde{K}$, then g, $S + h\cdot\mathrm{id}$ satisfy the Gauß-Codazzi equations for a surface of constant mean curvature h in a space of constant curvature $\tilde{K} - h^2$. He used this to construct constant mean curvature surfaces in $\mathbf{R}^3$, and exploited the fact that geodesics, which are curvature lines, i.e., (spherically) planar geodesics on the minimal surface, continue to be planar geodesics on the constant mean curvature surface, i.e., lines of fixed points of a reflectional symmetry.

We rephrase his result for S^3: If g, S are the metric and Weingarten map for a minimal surface in S^3, then $\cos^2\varphi \cdot g$, $(S + \sin\varphi \cdot \mathrm{id})/\cos\varphi$ are the local data of a surface of constant mean curvature $\tan\varphi$ in S^3 for which the same geodesics as for the minimal surface are spherically planar. Since the

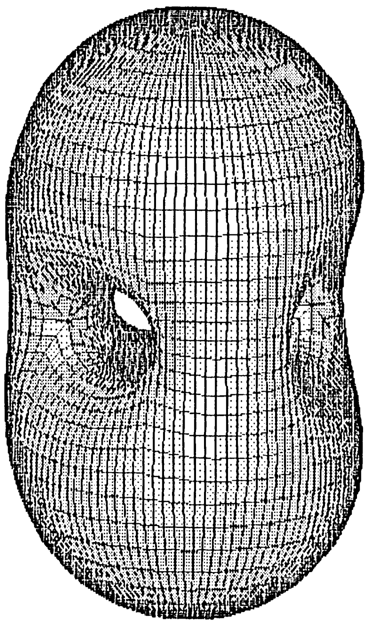

FIGURE 18

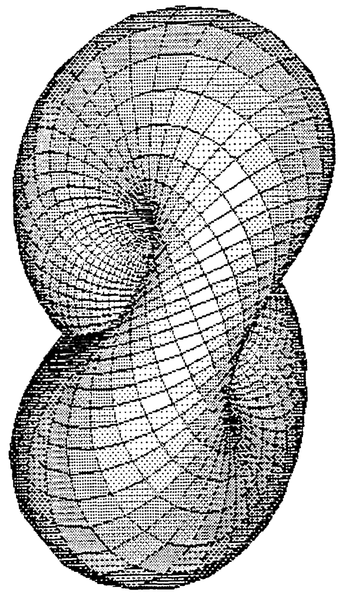

FIGURE 19

turning angle of these planar geodesics depends continuously on $\tan\varphi$, from the degree argument in the proof of our theorem we also get the existence of closed surfaces of constant mean curvature $\tan\varphi$ for small ϑ.

References

[1] P. Buser & H. Karcher, *Gromov's almost flat manifolds*, Astérisque **81** (1981).

[2] W. Y. Hsiang & H. B. Lawson, Jr., *Minimal submanifolds of low cohomogeneity*, J. Differential Geometry **5** (1971) 1–38.

[3] H. Karcher, *Schnittort und knovexe mengen in vollständigen Riemannschen Mannigfaltigkeiten*, Math. Ann. **177** (1968) 105–121.

[4] R. Kusner & U. Pinkall, *Some area estimates for surfaces with applications to the Willmore Problem*, in preparation.

[5] H. B. Lawson, Jr., *Complete minimal surfaces in S^3*, Ann. of Math. (2) **92** (1970) 335–374.

[6] ——, *The global behavior of minimal surfaces in S^n*, Ann. of Math. (2) **92** (1970) 224–237.

[7] W. H. Meeks III, *A survey of the geometric results in the classical theory of minimal surfaces*, Bol. Soc. Brasil. Mat. **12** (1981) 29–86.

[8] B. Smyth, *Stationary minimal surfaces with boundary on a simplex*, Invent. Math. **76** (1984) 411–420.

[9] S. T. Yau, *Problem Section, Seminar on differential geometry*, Annals of Math. Studies No. 102, Princeton University Press, Princeton, 1982, 669–706.

UNIVERSITY OF BONN

TECHNICAL UNIVERSITY OF BERLIN